JOURNAL OF COMPUTATIONAL PHYSICS 71, 34–49 (1987)

Phase-Change Simulation in a Propagative Medium Subject to a Heat Flux Disturbance

J. PAKLEZA

C.N.R.S., Laboratoire d'Informatique pour la Mécanique et les Sciences de l'Ingénieur, L.I.M.S.I., 91406 Orsay, France

AND

D. GENTILE

École Nationale Supérieure des Techniques Avancées E.N.S.T.A., Groupe Phénomènes d'Interface, 91120 Palaiseau, France

Received January 22, 1986; revised July 30, 1986

For very short transients or at very low temperature, the classical heat diffusion phenomenon breaks down because of the presence of temperature travelling waves which predominate on the energy transport. To take into account the above breakdown process, the usual parabolic equation for heat transfer can be substituted by a hyperbolic equation describing the temperature evolution in the medium. In this article numerical simulation of the latter is presented and the influence of the propagation of temperature waves on the liquid–vapour change is demonstrated. © 1987 Academic Press, Inc.

I. INTRODUCTION

Transient heat transfer problems are commonly solved by using the classical heat conduction equation

$$\frac{\partial T}{\partial t} = \alpha \frac{\partial^2 T}{\partial x^2},$$

which is a consequence of Fourier's law

$$Q = -k \frac{dT}{dx}$$

(in a one-dimensional situation). Consequently the speed of the propagation of a thermal disturbance is infinite, that is, the disturbance at any point will be instantaneously felt at every other point of the medium. This is known as heat conduction paradox [1, 2].

While in most practical cases, this description of the thermal behaviour of the medium is accurate enough; difficulties arise in situations where transients are very

0021-9991/87 $3.00

short (a few microseconds) or temperatures are very low (near absolute zero). Very short transients occur in particular in pulsed laser application technology [14–16]. Very low temperature operation is common in the case of liquid helium used as a refrigerant for cooling large superconductive coils through small channels.

These remarks led several authors [5] to introduce a modified Fourier's law which takes into account a relaxation time or build-up period for the establishment of a heat flow resulting from a thermal disturbance. This model implies that the temperature evolution follows a hyperbolic-type equation, with a finite speed of propagation, called "second sound velocity" in superfluid helium [6].

We have solved numerically recently [7, 8] the complete thermodynamics equations for Helium II given in [9, 10], calculated the relaxation time τ_c and showed that it is proportional to Q^{-2}. As a consequence for heat flux disturbances shorter than τ_c, the main character of the medium is propagative. On the contrary for longer duration than τ_c, the diffusive character is predominant and prevents propagative waves to develop inside the medium (Fig. 1). In fact, the description for superfluid helium is more complex because the entropy is transported with the normal fluid velocity V_n, according to the two-fluid model [11].

Thus, the simplified hyperbolic equation is valid only if the transport at V_n can be neglected as compared to the diffusive phenomenon. This is clearly demonstrated by performing an analysis of the non-dimensionalized equations [12].

In this work, we extend our previous simulation of energy transport in the case of a single liquid phase [7] to the liquid–vapour phase change and applied the results to Helium II looking, in particular, to conditions leading to a sudden phase change which in turn produces a temperature rise (burnout).

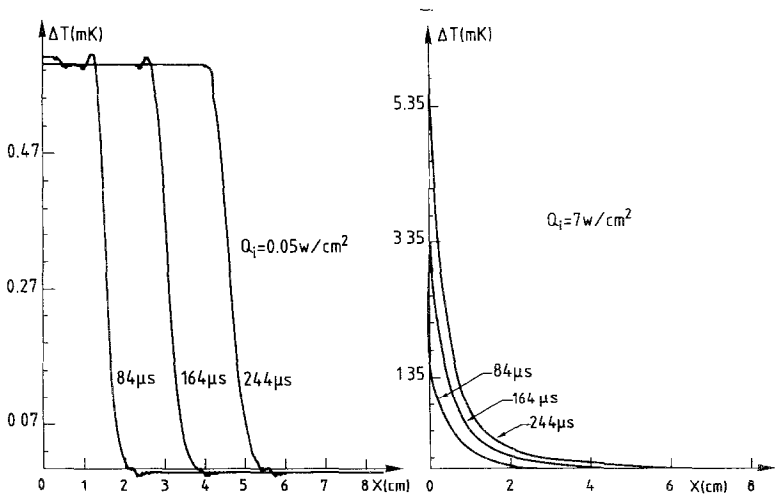

FIG. 1. Temperature profiles in two extreme cases of heat flux.

2. Mathematical Formulation of Phase Change

2.1. *The Non-linear Equations*

The general form of the equations [7] reduces in the one-dimensional case, in the absence of forced convection, to the three coupled non-linear equations

$$\frac{\partial T}{\partial t} = A\frac{\partial^2 T}{\partial x^2} + B\frac{\partial T}{\partial x} + CT + D \tag{1}$$

$$\frac{\partial V_n}{\partial t} = E\frac{\partial^2 V_n}{\partial x^2} - V_n\left[3\frac{\partial V_n}{\partial x} + FV_n^3\right] + G \tag{2}$$

$$\frac{\partial \theta}{\partial t} = \frac{k_v}{\rho_v C_v}\frac{\partial^2 \theta}{\partial x^2}, \tag{3}$$

where the coefficients A, B, C, D, E, F, G are functions of T and V_n through the physical variables such as entropy, specific heat, normal and superfluid density, viscosity and k_v, ρ_v, C_v are functions of temperature.

2.2. *Boundary and Initial Conditions*

2.2.1. At time $t = 0$ vapour is absent and the liquid phase is at rest, so the temperature is constant which implies:

$$(dT/dx)_{t=0} = 0$$

and the normal velocity component

$$V_n(x, 0) = 0.$$

2.2.2. At $x = L$ (free extremity of the channel), the boundary conditions are

$$T(L, t) = T_o \qquad \text{and} \qquad (dV_n/dx)_{x=L} = 0.$$

Since previous numerical experiments have demonstrated that the solution of the coupled equations set is completely independent of the boundary value of V_n, thus we take

$$V_n(0, t) = 0.$$

Since the liquid–vapour interface is taken at $x = 0$, the temperature boundary conditions are of 2 types:

— Neuman type if $T(0, t) < T_{sat}$ (liquid phase without vapour). In this case, the heat power Q_i is given and $T(0, t)$ is calculated as described in [7].

— Dirichlet type if $T(0, t) > T_{sat}$. In this case, the liquid–vapour phase change starts at $x = 0$ and the boundary condition (Fig. 2) becomes

$$T(0, t) = \text{Tsat}.$$

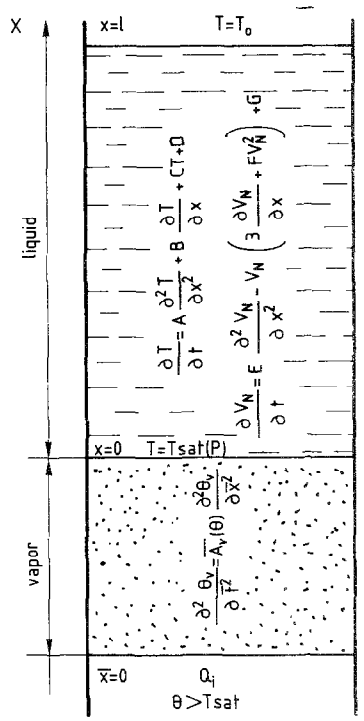

FIG. 2. Domains of resolution and boundary conditions.

2.2.3. There are no real initial conditions for the vapour phase, because, at the beginning of the simulated vapour formation, the vapour layer thickness, SEPS(0), is zero. If, in the following time-step Δt, SEPS(t) increases of the quantity EPS($t + \Delta t$), the initial temperature is thus imposed, equal to T_{sat} in this layer.

2.3. *Coupling Conditions*

Two different types of coupling can be noted:

— The first type concerns the variables $T(x, t)$ and $V_n(x, t)$, and their derivates $\partial T/\partial x$, $\partial T/\partial t$, $\partial V_n/\partial x$, $\partial V_n/\partial t$ [8].

— The second type concerns the liquid–vapour interface and corresponds to the strict identity of the temperatures (Fig. 2),

$$T(1, t) = \theta(m, t) = T_{sat}$$

and to the heat energy conservation (Fig. 3),

$$Q_o = Q_v + Q_{cr}. \tag{4}$$

The critical heat flux Q_{cr} corresponds to the amount of heat necessary to maintain the interfacial temperature equal to T_{sat} for the two following time-steps ($k * \Delta t$

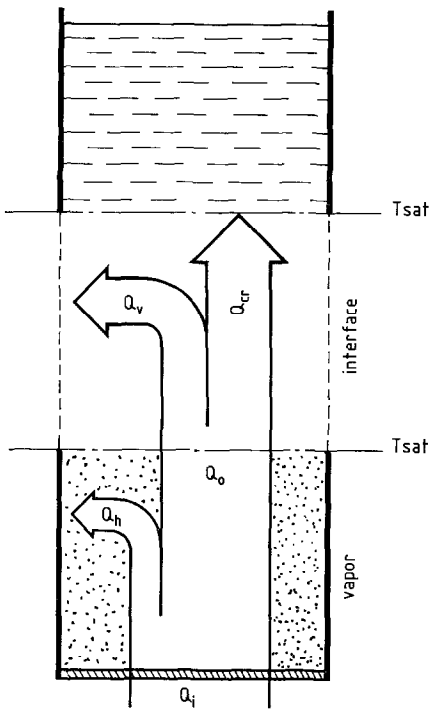

FIG. 3. Energy balance at the vapour–liquid unterface.

and $(k+1)*\Delta t)$. Its value depends on the solution for $T(x, t)$, $V_n(x, t)$ and $T(x, t+\Delta t)$, $V_n(x, t+\Delta t)$. Under the assumption that the interface temperature must be constant and equal to T_{sat}, the critical heat flux is calculated iteratively, with respect to the liquid boundary condition

$$T(0, t+\Delta t) = T(0, t) = T_{sat}.$$

3. NUMERICAL ALGORITHM

The proposed numerical simulation is based on the calculation of the variation of the vapour film thickness such as $T(x, t+\Delta t)$ and $\theta(x, t+\Delta t)$ are the unique solutions of Eqs. (1), (2), and (3) in accordance with the coupling condition (4) at the liquid–vapour interface. The complex iterative process of calculation leads, for every time-step, to find the value of $EPS(t+\Delta t)$. The convergence of the solution can be obtained for negative or positive values of $EPS(t+\Delta t)$, which corresponds either to a condensation or a vaporization process

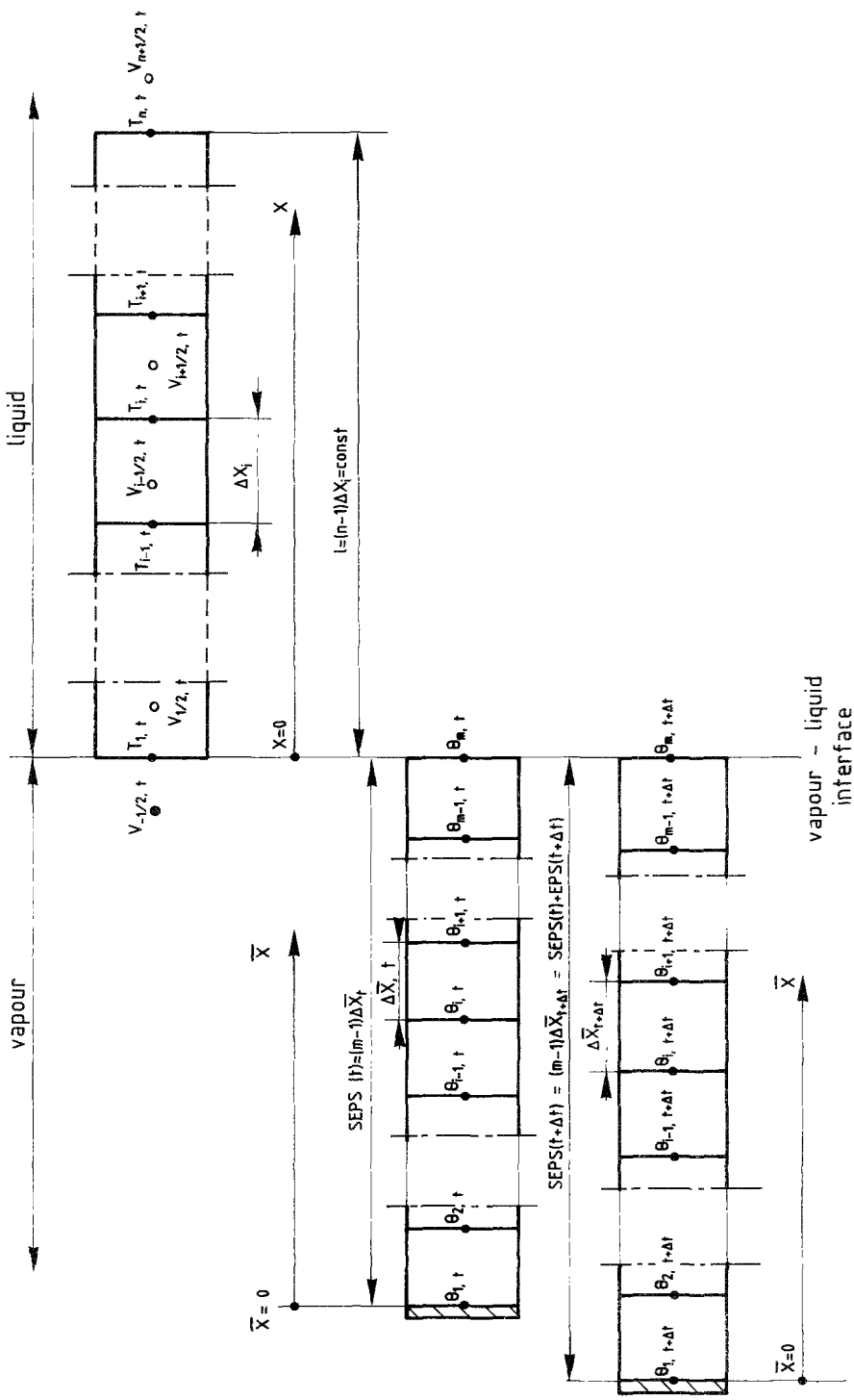

FIG. 4. Discretisation scheme for the liquid and vapour phase.

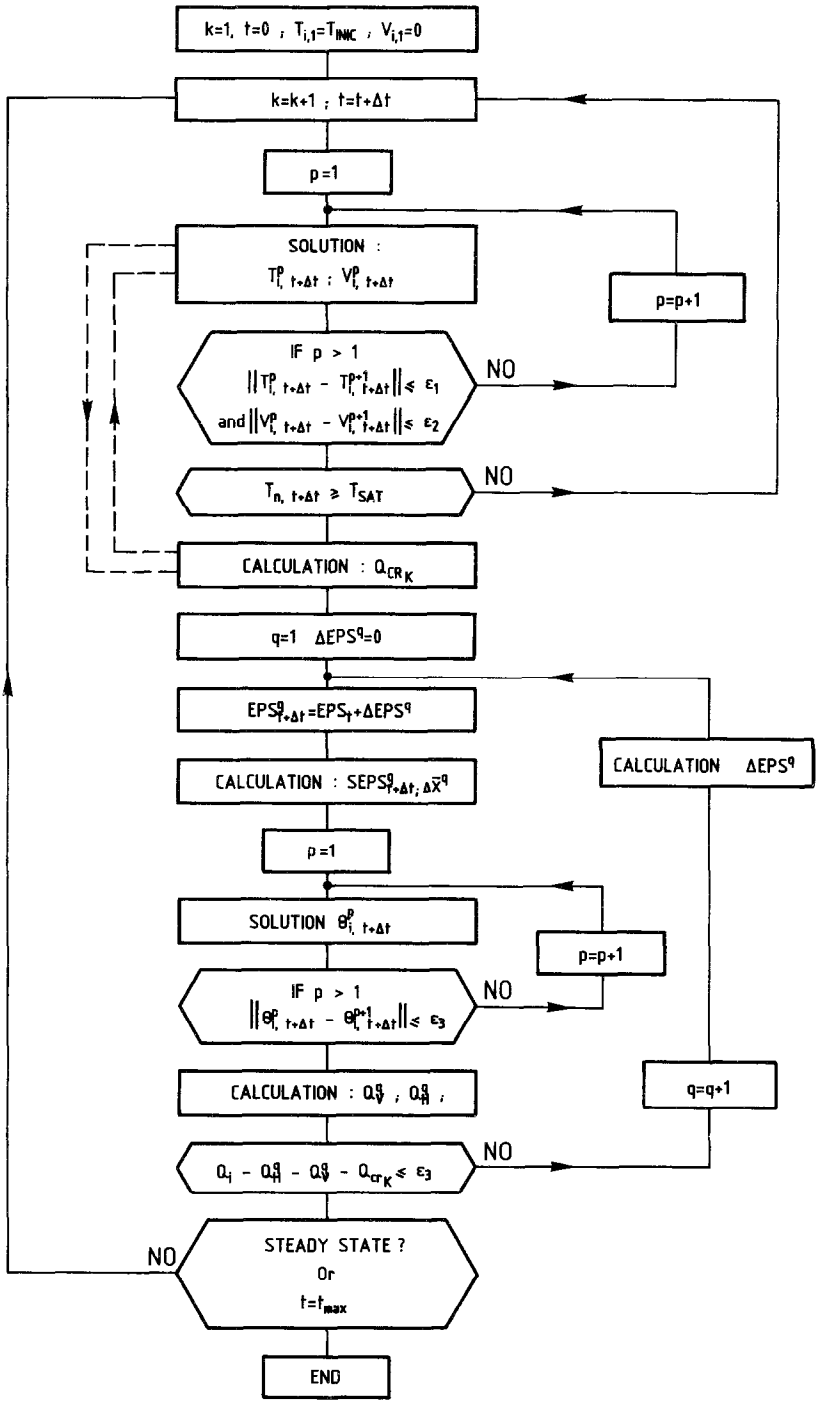

FIG. 5. Numerical algorithm.

In addition to a purely conductive heat transfer in the vapour phase, two other assumptions are made:

— The vapour pressure is constant at every point of the vapour layer.

— The interface thickness is zero (Figs. 3 and 4).

The vapour layer space discretisation is quite complex: the space-step $\Delta\bar{x}$ changes at every time-step but also it is modified during the iterative process inside a calculated time-step (Fig. 4).

The numerical algorithm is presented on Fig. 5, where the three iteration subloops inside the main time-step loop are shown. The first subloop is concerned with the solution of Eqs. (1) and (2) for the liquid. If the temperature $T(n, t+\Delta t)$ is smaller than T_{sat}, the calculation continues for the following time-step. But if $T(n, t+\Delta t) = T_{sat}$, the critical heat flux is calculated and its value stored.

Then $\mathrm{EPS}(t+\Delta t)^{q=1}$ is evaluated in the second subloop making possible the discretisation of the vapor layer and the initialisation of the $\theta(i, t)$ values.

The solution of $\theta(i, t+\Delta t)^{q=1}$ can also be obtained. $\mathrm{EPS}(t+\Delta t)^{q+1}$ is now evaluated by an iterative process up to the establishment of the convergence criterium

$$0 < \mathrm{ABS}(Q_i - Q_n^{q+1} - Q_v^{q+1} - Q_{cr}) < \varepsilon, \tag{5}$$

where ε is the admissible error of calculation. The third subloop, which is inside the second one, permits obtaining the vapour temperature solution $\theta(i, t+\Delta t)$ from the non-linear equation (3).

When (5) is satisfied, the calculation starts again for the following time-step or stops if the stationary regime has been reached.

The different calculations have been made with the space discretisation $0.01 < \Delta x/L < 0.1$ for the liquid and $\Delta\bar{x}/L = 0.1$ for the vapour phase. In order to reach a good convergence, the following inequality $\Delta x/\Delta t > 40$ has been respected, as mentioned by the authors in [7]. Generally, the number of iterations necessary to solve $T(x, t)$, $V_n(x, t)$, and $\Theta(x, t)$ and for satisfying the energy balance have been smaller than 10 for every time-step. The relative values of stop-tests are fixed to 10^{-5}.

Calculations have been performed on the NAS9080 computer of the Circe Center of C.N.R.S. at Orsay. Double precision mode of calculation took about 90 sec for 400 time-steps.

4. Results Presentation and Discussion

5.1. *General Behavior*

Figure 6 illustrates the general behaviour of the numerical model in the conditions

$$Q_i = 1.46 \text{ W/cm}^2$$

$$T_o = 1.80 \text{ K}$$

$$L = 8.5 * 10^{-3} \text{ m}$$

$$\Delta\text{Tsat} = \text{Tsat} - T_o = 40 \text{ mK}.$$

Because of the very low value of the temperature gradients in superfluid helium (due to its high thermal conductivity), all the results are represented by the relative temperature variation $\Delta T(x, t)$ which is the difference between the absolute value of the temperature $T(x, t)$ and the constant reference temperature T_o at $x = L$.

The temperature profile $\Delta T(x)_t$ along the channel in the liquid phase is represented on Fig. 6a for different times. Figure 6b corresponds to the temperature evolution with time at different stations in the liquid channel. The evolution of the vapour layer thickness versus the time is shown in Figs. 6c and d is the vapour formation velocity.

These results show the possible existence of a spatial and temporal stationary interface as demonstrated by the temperature profile $\Delta T(t)_x$ and $\Delta T(x)_t$ and achieved for a heat flux value slightly greater than 1.40 W/cm^2 (solution of the permanent regime in the single liquid phase corresponding to a constant temperature gradient),

$$\nabla T = \frac{T_{x=0} - T_{x=L}}{L}$$

with

$$T_{x=0} = \left(1 - \frac{\rho_L L g}{L_{\text{th}} \rho_v}\right)$$

calculated from the linearized Clausius-Clapeyron equation.

The vaporization process takes place in less than 1 ms and is associated with a temperature disturbance propagating through the liquid phase at the second sound velocity. This result was experimentally observed and reported in [17]. Figure 7 shows the record of the temperature perturbation detected at 0.5 cm from the heater in a He II channel for two bath temperatures (2.1° K, Fig. 7a and 1.8° K, Fig. 7b). This indicates that vaporization can be associated to a transient cooling of the liquid [18]. The vaporization speed is very high and it should be pointed out that its time change corresponds to an acceleration of about 100 g. As the vapour layer is stabilized, the vaporization speed falls to zero.

5.2. *Effects of the Propagation, Pseudo-Diffusion and Convection Terms*

These effects are illustrated on the Figs. 8, 9, and 10.

5.2.1. Vapour thickness evolution versus time due to a heat flux of 1.46 W/cm^2 in the two following cases:

— Figure 8a corresponds to the numerical solution of the complete set of coupled equations (1) and (2) as described previously in Section 2. A stable interface can be reached.

— Figure 8b corresponds to the solution of the equations set but only with the diffusion term. The propagation and convection terms have been eliminated in

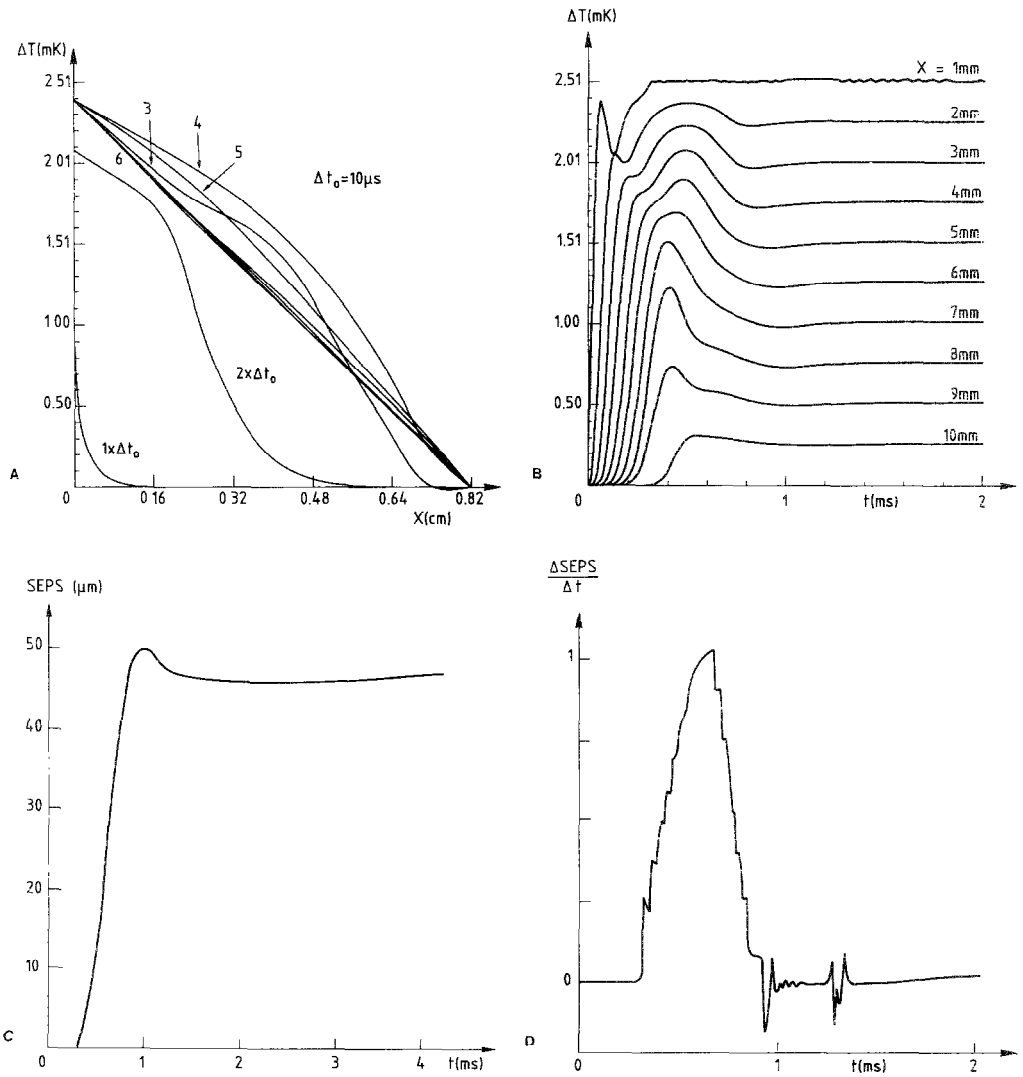

FIG. 6. (a) Temperature profile for different times. (b) Temperature evolution at different stations. (c) Vapour thickness evolution. (d) Vapour formation velocity with time.

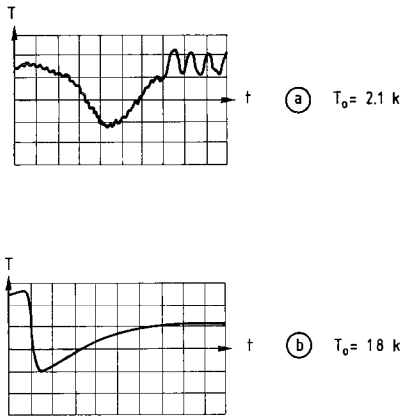

FIG. 7. Temperature perturbation in the liquid detected experimentally at the time of phase transition (not scaled).

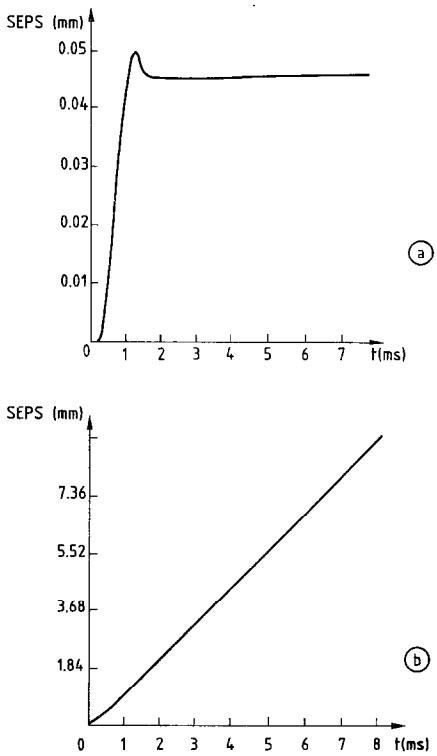

FIG. 8. (a) Vapour thickness evolution in the general case for a heat flux of 1.46 W/cm^2. (b) Idem (a) in the case of a pure diffusion process.

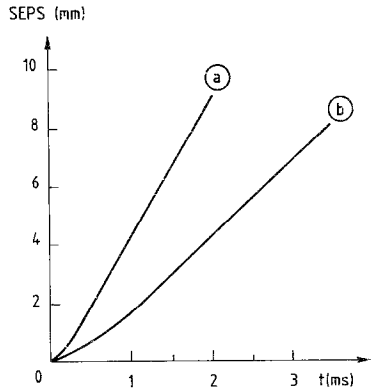

FIG. 9. (a) Vapour thickness evolution in the general case for a heat flux of 7.0 W/cm^2. (b) Idem (a) in the case of a pure diffusion process.

order to take into account the pure diffusion process. It should be pointed out that in the case of single diffusion and for the same boundary conditions, the stability of the interface is not possible, the vapour thickness increases continuously with time.

5.2.2. Idem 5.2.1 for a heat flux $Q_1 = 7$ W/cm^2 (diffusive process of heat transport only [7]).

— Figure 9a illustrates the vapour evolution in the same case as Fig. 8a, i.e., it corresponds to the solution of Eqs. (1) and (2) for the liquid.

— Figure 9b is similar to the result of Fig. 8b, i.e., the solution is obtained by taking off the propagation and convection terms of Eqs. (1) and (2).

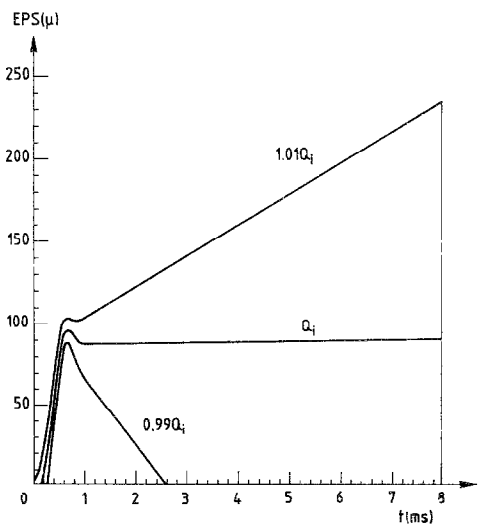

FIG. 10. Conditions of the interface stability.

The behaviour of the vapour interface is quite similar in these two cases, except for a change in the slope $d(\mathrm{SEPS})/dt$. This change can be related to the presence of the convection term in the case of Fig. 9a, which corresponds to the entropy transport at V_n. This term does not exist indeed in the pure diffusive case of a normal fluid.

5.2.3. Figure 10 demonstrates the influence of small perturbations on the stability of the interface. It should be noted that a variation of about 1% of the heat flux Q_i (or of the hydrostatic pressure) breaks the equilibrium and starts the vaporization of the condensation depending on the heat flux modification with respect to the equilibrium value. Also, the process of condensation or vaporization can alternate with a well-determined oscillation frequency. This result seems to be due to the predominance of the propagation terms in the equations. Numerical and experimental work is in progress to investigate this phenomenon more accurately.

5.3. *Interpretation*

In order to interpret the present results, let us consider the time evolution of the heat fluxed on the interface which satisfy the energy balance condition

$$Q_v + Q_{cr} + Q_h = Q_i = \text{const.}$$

Figure 11 shows Q_o and Q_{cr} as a function of time for the cases corresponding to Figs. 8a, b and 9b.

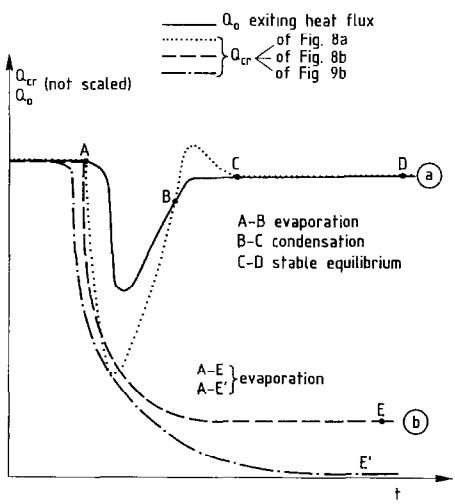

FIG. 11. Heat fluxes evolution at the liquid–vapour interface.

For the diffusive or the pseudo-diffusive mode (transport at V_n) the temperature increase in $X=0$ is related to the heat flux by

$$\Delta T_{x=0} = \frac{Q_{cr} t^{1/2}}{A},$$

where A is a constant.

As $T(0, t) = T_{sat}$ is imposed, Q_{cr} decreases continuously as $t^{-1/2}$ (AE' in Fig. 11). However, it reaches a limiting value $S * T_o * V_n * \rho_l$ in the case of a pseudo-diffusive transport mode (AE in Fig. 11).

When the vaporization process starts, Q_h increases and Q_o decreases, as a result of the heating of the vapour. Then Q_o increases to reach the stationary regime, where $Q_h = 0$ ($Q_o = Q_i$).

This case is clearly shown in Fig. 11, where $Q_v = Q_o - Q_{cr} = \text{const.}$ The vaporization process does not stop and the vapour thickness increases linearly with time.

For the predominant propagative mode, Q_v and Q_h increase while Q_{cr} decreases. In this case

$$\Delta T_{x=0} = \frac{Q_{cr}}{\rho_L c_L u_2},$$

where u_2 is the "second sound velocity."

Since T must be maintained equal to $T_{sat} = \text{const.}$, Q_{cr} must increase again as shown in Fig. 11 ($ABCD$ in Fig. 11). The propagation term decreases, according to the conclusions of [7], up to the stationary regime. Depending on the value of T_{sat} the flux Q_{cr} can reach a value smaller, equal, or greater than Q_o. That explains the results on Figs. 8a and 9.

Conclusions

The influence of the propagation of temperatures waves on the phase change of superfluid helium has been clearly demonstrated through an accurate numerical simulation. In particular, the possible existence of a stable liquid–vapour interface has been directly related to the propagative character of the medium. The practical consequences can be drastic. Indeed, in the pure diffusive case (solution of the classical heat conduction equation without propagative terms), the temperature at the wall can increase up to 7000 K, while the propagation limits this temperature increase to about 400 K for a calculated vapour film thickness of 70 μ.

Consequently, it will always be better to evacuate the heat energy $Q * t$ by the propagative mode and not by the diffusive one. Thus, it will be preferable to work at small values of flux Q during long times t, since propagation vanishes in the medium as Q^2. This operation mode corresponds to an appropriate design of the

heater surface and the heat exchange area. The numerical model can contribute to optimize the design procedure in applications such as refrigeration of superconductors, thermostabilisation, etc.

Even if the model does not take into account eventual dynamical effects such as a possible overpressure in the vapour phase and pressure discontinuities at the interface of phase change, its use is still valid since these effects are limited to very short times after the beginning of vaporization. A more elaborate mathematical and numerical model is now in progress to take into account the effect of bidimensional geometries and the dynamical effect.

APPENDIX: NOMENCLATURE

A, B, C, D, E, F — equations coefficients
EPS — vapour thickness variation
L — length
Q — heat flux
S — entropy
SEPS — vapour thickness
T — liquid temperature
V — velocity

c — specific heat
d — diameter, derivative
g — gravity
i, k — current index
k — thermal conductivity
m, n — number of nodes
t — time
x, x — space coordinate

α — thermal diffusivity
∂ — partial derivative
ρ — density
τ — characteristic time
Δ — variation operator
θ — vapour temperature

INDEX:

cr — critical value
h — for heating
i — input
l — liquid
n — normal component
o — out
p, q — number of iteration
s — superfluid component
sat — saturation
v — vapour

ACKNOWLEDGMENT

This work has been financially supported by a PIRSEM-CNRS A.T.P. contract.

REFERENCES

1. C. CATTANEO, *C.R. Acad. Sci. Paris* **247**, 431 (1952).
2. P. VERNOTTE, *C. R. Acad. Sci. Paris* **246**, 3154 (1958).
3. V. PESHKOV, *J. Phys. USSR* **8**, 381 (1944).
4. W. F. VINEN, *IIF-IIR Bul. Refrig. Sci. Technol.*, 256 (1981).
5. P. M. MORSE AND H. FESHBACH, *Methods of Theoretical Physics* (McGraw–Hill, New York, 1953).
6. R. B. DINGLE, *Proc. Phys. Soc. A* **63**, 638 (1950).
7. D. GENTILE AND J. PAKLEZA, *Numer. Heat Trans.* **6**, 317 (1983).
8. D. GENTILE AND M. X. FRANCOIS, "Transport d'énergie dans l'hélium superfluide", in *6ème Congrés Français de Mécanique*, Lyon, September, 1983.
9. I. M. KHALATNIKOV, *Introduction to the Theory of Superfluidity* (Benjamin, New York, 1965), p. 55.
10. D. LHUILLIER, in *Proceedings of 14th International Congress of Theoretical and Applied Mechanics, Delft, The Netherlands*, 1976.
11. LD. LANDAU, *J. Phys. USSR* **5**, 71 (1941).
12. D. GENTILE AND J. PAKLEZA, "An Analytical and Numerical Investigation of Heat Transport in Superfluid Helium." *XVII Biennial Fluid Dynamics Symposium, Poland, September 1, 1985.*
13. R. AYMAR ET AL., *IEEE Trans. Magn.* **17**, 38 (1981).
14. K. J. BAUMEISTER AND T. D. HAMIL, *J. Heat Transfer* **91**, 543 (1969).
15. V. A. BUBNOV, *J. Heat Mass Trans.* **19**, 1975 (1976).
16. M. N. OZISIK AND B. VICK, *Int. J. Heat Mass Transf.* **27**, 1845 (1984).
17. D. GENTILE AND M. X. FRANCOIS, *Cryogenics* **21**, 234 (1981).
18. D. A. LABUNTZOV AND E. V. AMETISTOV, *Teploenergetika* **27**, 60 (1980).